# Effect of alkali metal perchlorate and iodate type on boron ignition: The role of oxidizer phase change

Yujie Wang [a], Haiyang Wang [a], Feiyu Xu [a,b], Pankaj Ghildiyal [a,b], Michael R. Zachariah [a,*]

[a] Department of Chemical and Environmental Engineering, University of California, Riverside, CA 92521, United States
[b] Department of Chemistry and Biochemistry, University of Maryland, College Park, MD 20742, United States

ABSTRACT

Boron often demonstrates low reactivity despite having high gravimetric and volumetric energy density. Here we explore a family of oxidizers with very similar chemistries to understand controlling mechanisms in boron ignition. Alkali metal perchlorates as well as iodates ($LiClO_4$, $NaClO_4$, $KClO_4$, $LiIO_3$, $NaIO_3$ and $KIO_3$) were investigated under rapid heating conditions ($\sim 10^5$ K/s) by temperature-jump (T-Jump) ignition and time-of-flight mass spectrometry (TOFMS). T-Jump ignition tests in atmospheric pressure argon show that $B/LiClO_4$, $B/NaClO_4$, $B/LiIO_3$, and $B/NaIO_3$ ignite while $B/KClO_4$ and $B/KIO_3$ do not, despite the near identical chemistries. T-Jump TOFMS results demonstrate a dramatic increase of Cl and I containing species for Li and Na systems relative to K when B is added. Thermogravimetry/differential scanning calorimetry (TGA/DSC) analysis reveals that there is a temperature gap between melting and decomposition onset of $LiClO_4$, $NaClO_4$, $LiIO_3$, and $NaIO_3$, respectively, whereas $KClO_4$ and $KIO_3$ melt and decompose concurrently. We find that the larger interval between melting and decomposition renders more time for the oxidizer to melt and surround/wet the nanoscale B before decomposing, providing instant access to oxygen for B nanoparticles that results in vigorous ignition. This study of a set of equivalent oxidizers illustrates the important role of transport phenomena and physical properties have on ignition.

## 1. Introduction

Nanoscale particles including boron, aluminum, titanium, silicon, and zirconium have been the focus of research for energetic materials including propellants and pyrotechnics due to their potential as high energy density fuels [1–5]. Of these boron has always been ranked as the most attractive due to its very high gravimetric and volumetric energy content [6–8]. However it is well known that boron suffers from slow oxidation kinetics since its native oxide shell boron oxide ($B_2O_3$) has a low melting point (723 K) and a high boiling point (2130 K) [9], leading to a liquid barrier that retards the reactivity [6–8,10–13]. Another limiting factor is the lowered energy release from combustion of boron in hydrogen containing gases due to the thermodynamically favored formation of HOBO, which "traps" boron and prevents it from forming gaseous $B_2O_3$ and releasing all its potential energy [8,14]. To overcome the challenge from the low reactivity of boron, various approaches have been investigated, including washing to dissolve the oxide layer [15], using metal carbides for accelerating energy release [16], mixing boron with metal or metal hydride additives [17–24], decreasing the size of

boron particles to the nanoscale [25,26], coating boron particles with oxidants, metal fluorides, organics or polymers [3,27–35]. In addition to modifying boron particles, other studies have investigated tuning the ignition and combustion performance of boron using different solid-state oxidizers including metal oxides [9,36], binary metal oxides [9,37], metal oxides with oxygen vacancy [38,39], mixture of graphene oxide and graphite fluoride [40], as well as gaseous fluorine-based oxidizers [8,41]. Alkali metal perchlorates are attractive oxidizers for boron because of their higher oxygen content compared to commonly utilized metal oxides. Moreover, $B/MClO_4$ (M = Li, Na and K) reactions have much higher combustion enthalpies on both gravimetric and volumetric basis of boron than many common B/metal oxide systems (Fig. 1). Similarly, B with alkali metal iodates also have higher combustion enthalpies compared to B with these common metal oxide systems. However, the ignition mechanism of boron with these metal perchlorates and iodates as oxidizers have not been widely explored [42].

This article systematically investigates the ignition mechanism of boron nanoparticles with alkali metal perchlorates ($LiClO_4$, $NaClO_4$, and
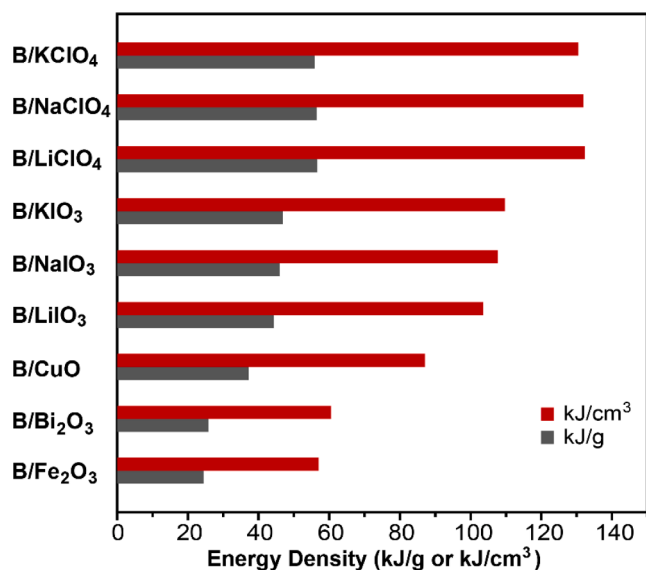
**Fig. 1.** Combustion enthalpies of boron with different oxidizers ($\Phi=1$) per g or cm$^3$ of boron [43].

KClO$_4$) and iodates (LiIO$_3$, NaIO$_3$, and KIO$_3$). Temperature-jump ignition (T-Jump ignition) tests and temperature-jump time of flight mass spectrometry (T-Jump/TOFMS) under rapid heating ($\sim10^5$ K/s) conditions were utilized to analyze ignition and reaction characteristics. Thermal decomposition of alkali metal perchlorates and iodates under slow heating (10 K/min) conditions were conducted with thermogravimetry–differential scanning calorimetry (TGA-DSC) to support the observations from T-Jump measurements. A mechanism explaining the observed ignition behavior difference among the B/MClO$_4$ as well as B/MIO$_3$ (M = Li, Na, K) composites is proposed.

## 2. Material and methods

### 2.1. Materials/Sample preparation

Nanoscale boron ($\approx$100 nm, $\sim$85% active) was purchased from US Research Nanomaterials, Inc. LiClO$_4$ (99%), NaClO$_4$ (>98.0%), KClO$_4$ (99%), NaIO$_3$ (99%) were purchased from Alfa Aesar. LiIO$_3$ (97%) and KIO$_3$ ($\geq$98%) were purchased from Sigma Aldrich (Millipore Sigma). μm-sized alkali metal perchlorates and iodates particles were synthesized via an aerosol spray pyrolysis (ASP) approach [44,45]. Generally, 1 g of as-purchased larger particles were dissolved into 100 mL of deionized water and the obtained solution was sprayed into small droplets with an atomizer that operated at $\sim$ 35 psi using compressed air. The droplets passed through a silica-gel diffusion drier to remove water and sequentially passed through a tube furnace that operated at 350 °C for LiClO$_4$ and NaClO$_4$, 150 °C for KClO$_4$, LiIO$_3$, NaIO$_3$ and KIO$_3$. The final product was collected on a filter paper.

### 2.2. Characterization

Particles sizes and morphologies of micron-sized alkali metal perchlorates and iodates particles from ASP were characterized by Scanning Electron Microscopy (SEM, FEI NNS450) operating at 20 kV. Active content of B nanopowder was determined with thermogravimetry and differential scanning calorimetry (TGA − DSC) using a Netsch STA449 F3 Jupiter thermal analyzer. Boron powder was loaded into an alumina crucible inside the instrument and heated to 1200 °C at a heating rate of 10 K/min under an oxygen flow of 50 mL/min with an additional isotherm at 1200 °C for 2 h. TGA − DSC tests for thermal decomposition of synthesized alkali metal perchlorates and iodates particles from ASP were conducted using a SDT Q600 from TA Instruments. Generally, the

powders were placed into alumina crucibles inside the instrument and heated to 600 or 700 °C under an argon flow of 100 mL/min. X-ray diffraction crystallography (XRD, PANanalytical Empyrean Series 2 diffractometer) was used to characterize the alkali metal perchlorates and iodates particles from ASP with Cu Kα radiation. As shown in Figure S3, the alkali metal perchlorate particles synthesized from ASP were LiClO$_4$·3H$_2$O, a mixture of NaClO$_4$·H$_2$O and NaClO$_4$, KClO$_4$, respectively. H$_2$O in LiClO$_4$·3H$_2$O was considered as an oxidizer for boron oxidation when calculating the equivalence ratio according to the following reaction equation (Equation (1)) due to its high content ($\approx$34% of total mass) [6,7]. For simplicity, LiClO$_4$·3H$_2$O will be referred to as LiClO$_4$.

$$\text{LiClO}_4\cdot3\text{H}_2\text{O} + 4\text{B} \rightarrow \text{B}_2\text{O}_3 + 2\text{HOBO} + 2\text{H}_2 + \text{LiCl} \tag{1}$$

H$_2$O in the mixture of NaClO$_4$·H$_2$O and NaClO$_4$ from ASP was not considered due to its low content ($\approx$3% of the total mass), as shown in Fig. 4. Equation (2) was used when calculating the equivalence ratio for boron with NaClO$_4$ and KClO$_4$.

$$3\text{AClO}_4 + 8\text{B} = 4\text{B}_2\text{O}_3 + 3\text{ACl} \tag{2}$$

where A = Na and K. Two equivalence ratios mainly, $\Phi=1$ and 1.5, were studied for the three boron/ alkali metal perchlorate systems. Higher equivalence ratios were also studied for B/LiClO$_4$.

XRD results showed the alkali metal iodate particles from ASP were LiIO$_3$, a mixture of NaIO$_3$·H$_2$O and NaIO$_3$, KIO$_3$, respectively, as show in Figure S5. H$_2$O in the mixture of NaIO$_3$·H$_2$O and NaIO$_3$ was not considered for calculating the equivalence ratio due to the low content (<3%) (Fig. 6). Equation (3) was used to determine the equivalence ratio for boron and alkali metal iodates.

$$\text{MIO}_3 + 2\text{B} = \text{B}_2\text{O}_3 + \text{MI} \tag{3}$$

where M = Li, Na and K. One equivalence ratio, $\Phi=1.5$, was studied for boron/alkali metal iodate systems.

### 2.3. T-Jump Ignition and T-Jump/TOFMS

The details of T-Jump ignition and T-Jump/TOFMS experiments and the operational settings can be found in previous publications from our group [44,46–49]. The composites were prepared by a physical mixing method. Generally, boron powder and corresponding amounts of oxidizers synthesized from ASP were suspended in hexane in a vial. After 30 mins of sonication, a small amount of the suspension was deposited on the Pt wire (diameter = 76 μm, 0.8–1.1 cm length, OMEGA Engineering Inc.) that was soldered between two copper leads of a T-Jump probe. The Pt wire was resistively heated by a direct current voltage supply that delivers a 3 ms pulsed square wave signal. Fast response thermometry of the Pt wire was acquired and temperature readings were obtained through the calibration relationship between the temperature of the Pt wire and its corresponding resistance from the Callendar-Van Dusen equation. The temperature of the thin coating on Pt wire was approximately the temperature of the wire. The measurements were repeated at least three times for one sample.

For T-Jump/TOFMS, mass spectrometry was obtained by using a trigger signal that communicates wire heating and collection of mass spectra simultaneously. A 70 eV electron gun ionization source was used to ionize gas phase species produced by sample heating. A Teledyne LeCroy 600 MHz oscilloscope was utilized to collect the raw data of mass spectra, current and voltage readings over a 10 ms collection period with 0.1 ms interval. For T-Jump ignition tests, the Pt wire was soldered on a different sample holder that is inserted into a chamber with inlets and outlets for flowing gases and vacuum, a pressure gauge as well as a glass window for imaging of the sample inside the chamber, as described with details in our previous studies [50,51]. The ignition delay time was determined from the video captured with high-speed camera (Vision Research Phantom V12.1). The ignition tests were conducted under 1
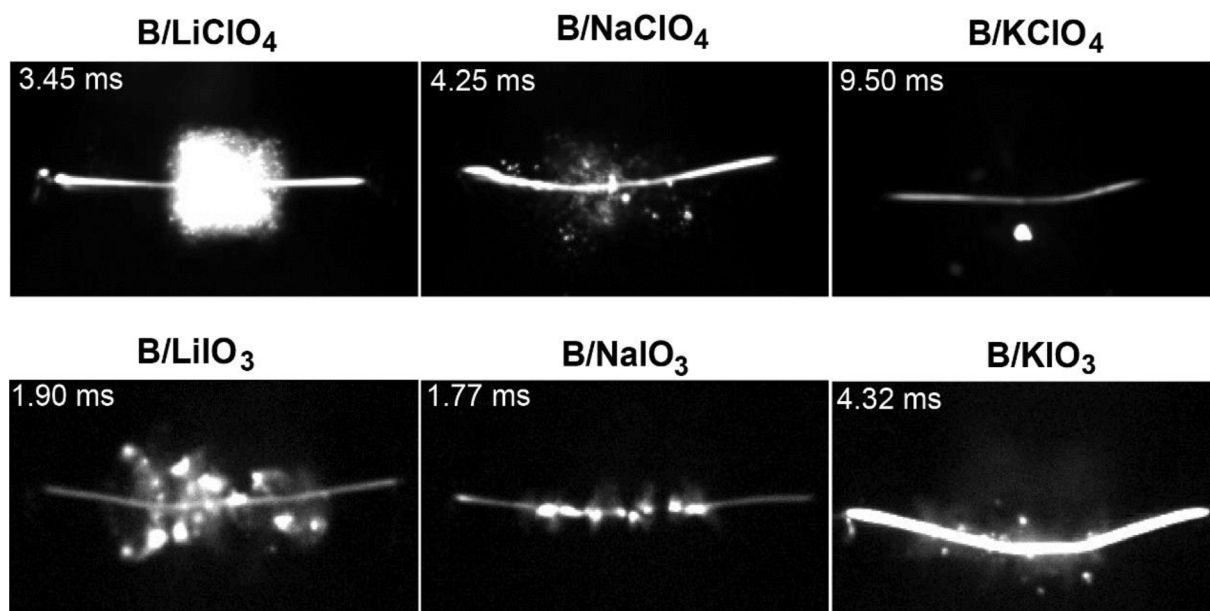
**Fig. 2.** T-Jump ignition snapshots of B with $LiClO_4$ (top left), $NaClO_4$ (top middle), $KClO_4$ (top right), $LiIO_3$ (bottom left), $NaIO_3$ (bottom middle) and $KIO_3$ (bottom right) with peak flame size in 1 atm argon, $\Phi=1.5$. The inserted time in every snapshot is the time after triggering. Note: B/perchlorate (top) snapshots have sensitivity of 1, B/iodate (bottom) snapshots have sensitivity of 16.
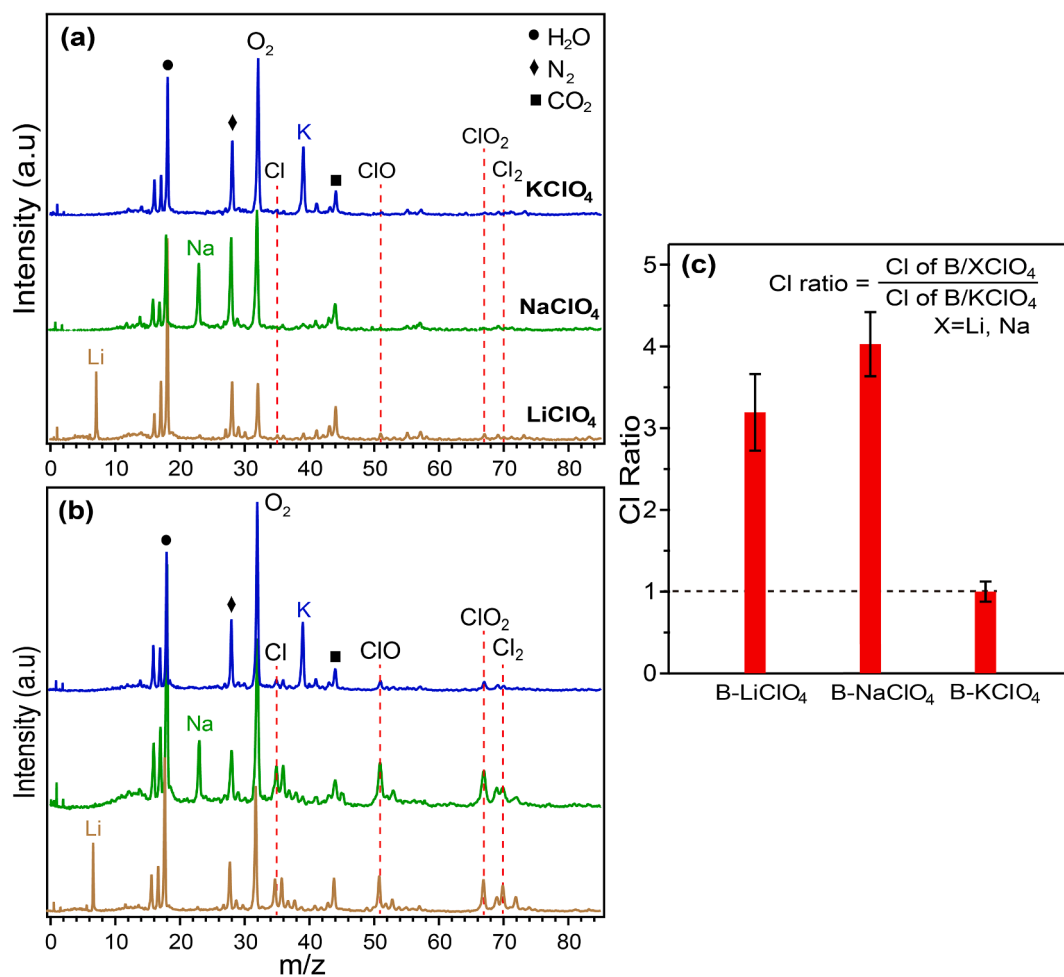


**Fig. 3.** Mass spectrum of rapidly heated $LiClO_4$ (bottom), $NaClO_4$ (middle), and $KClO_4$ (top) in (a), and the corresponding composites with B with $\Phi=1.5$ in (b). The spectra are normalized to the corresponding metal ion, and most notable mass species are labeled. (c) the measured relative Cl release of B-$XClO_4$ to the B-$KClO_4$, where X = Li, Na.
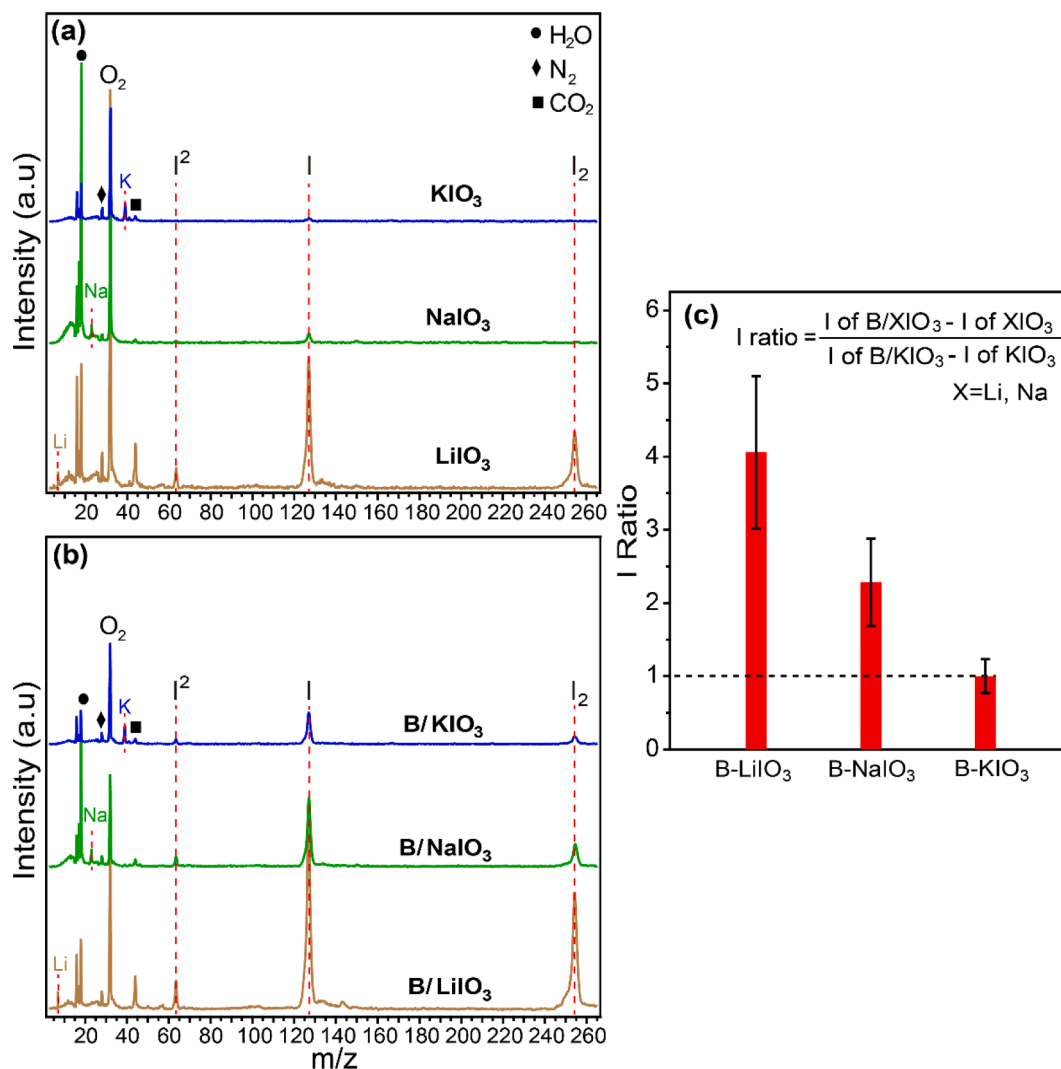
**Fig. 4.** Mass spectrum of rapidly heated $LiIO_3$ (bottom), $NaIO_3$ (middle), and $KIO_3$ (top) in (a), and the corresponding composites with B with $\Phi=1.5$ in (b). The spectra are normalized to the corresponding metal ion, and most notable mass species are labeled. (c) the measured relative Cl release difference between B-$XClO_4$ and $XIO_3$ to the difference between B-$KIO_3$ and $KIO_3$, where X = Li, Na.

atm argon.

## 3. Results and discussion

### 3.1. Ignition under rapid heating rate ($\sim 10^5$ K/s)

Ignition studies of boron with alkali metal perchlorates and iodates were conducted in 1 atm argon. The representative snapshots of ignition with $\Phi=1.5$ are shown in Fig. 2 and the progressions of ignition are shown in Figure S1 and S2. These results reveal that with $\Phi=1.5$, B/$LiClO_4$ and B/$NaClO_4$ ignite although B/$NaClO_4$ has a less vigorous flame, while B/$KClO_4$ barely ignites, even though some glowing particles are present. Similarly, B/$LiIO_3$ and B/$NaIO_3$ ignite while B/$KIO_3$ does not. This demonstrates a reactivity difference among these perchlorates as well as iodates acting as oxidizer for boron. We will explore the reasons for these differences in subsequent sections of this paper.

Figure S1 shows that B/$NaClO_4$ and B/$KClO_4$ maintain their ignition behavior as equivalence ratio changes from 1 to 1.5, however, B/$LiClO_4$ does not ignite at equivalence ratio of 1 although it ignites vigorously at equivalence ratio of 1.5 and higher equivalence ratios (Figure S7). As mentioned previously, XRD results (Figure S3) show that the particles synthesized from ASP of $LiClO_4$ is actually $LiClO_4 \cdot 3H_2O$, and we were unable to prepare a stable anhydrous sample. Therefore, $H_2O$ is

considered as an oxidizer in the equivalence ratio calculation as shown in Equation (1), although the exact reaction mechanism between B and $H_2O$ is not well understood [6–8,52–54]. The fact that B/$LiClO_4$ only ignites when fuel-rich (ignition snapshots of $\Phi=2$ and 3 are shown in Figure S7) suggests a different role of $H_2O$ than what is shown in Equation (1), but this is beyond the scope of this study.

One may surmise the ignition difference simply arises from the thermochemical property difference. But as shown in Fig. 1, there is no significant difference in reaction enthalpies among B/perchlorates as well as in B/iodates. Therefore, the ignition behavior difference cannot be explained by the thermochemical property of the reactions.

### 3.2. Reaction products under rapid heating rate ($\sim 10^5$ K/s)

T-Jump/TOFMS was utilized to analyze reaction intermediates and products of metal perchlorates as well as iodates with and without the presence of B under high heating rates ($\sim 10^5$ K/s). The resulting mass spectra summed over a collection period time of 10 ms at a 0.1 ms interval are displayed in Fig. 3 (a) and (b) as well as Fig. 4 (a) and (b).

The bare metal perchlorates have similar decomposition patterns, releasing the corresponding metal (Li, Na, K), $O_2$, as well as small amounts of Cl-containing species including Cl, ClO, $ClO_2$ and $Cl_2$. When B is introduced, the metal perchlorates behave differently, where the
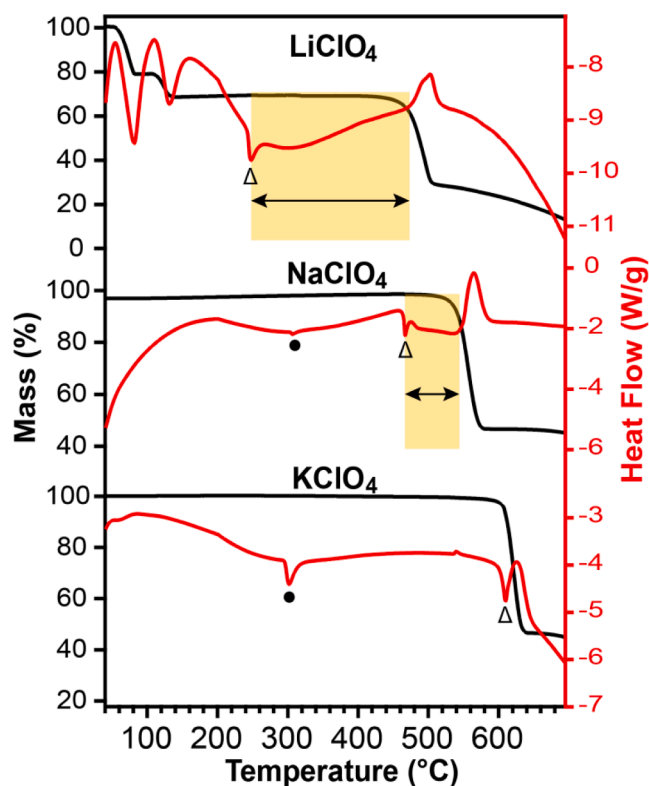
**Fig. 5.** TGA-DSC of $LiClO_4$ (top), $NaClO_4$ (middle) and $KClO_4$ (bottom) under argon environment. ● indicates phase transition and Δ indicates melting. The orange area indicates the temperature range from melting to decomposition onset.
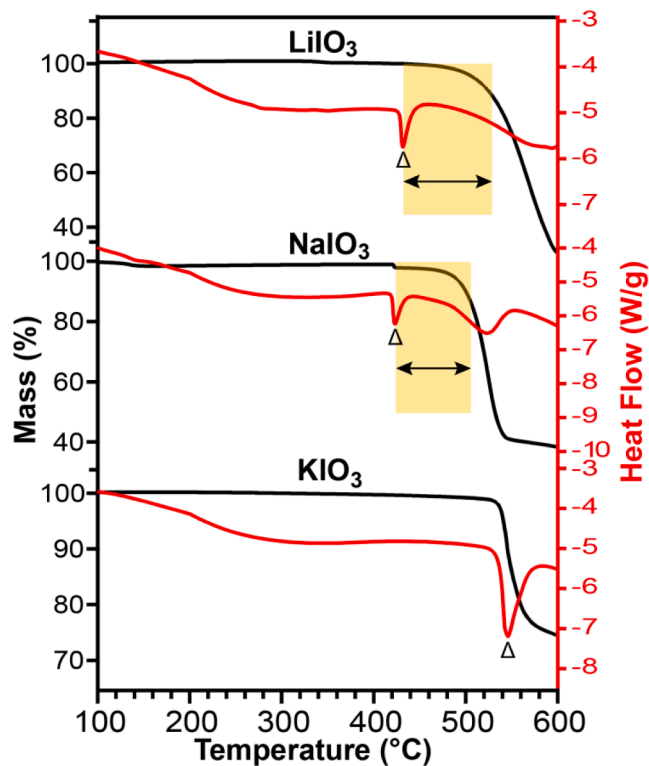


**Fig. 6.** TGA/DSC of $LiIO_3$ (top), $NaIO_3$ (middle) and $KIO_3$ (bottom) under argon environment. Δ indicates melting. The orange area indicates the temperature range from melting to decomposition onset.

intensity of the Cl-containing species dramatically increases for $LiClO_4$ and $NaClO_4$, however it only increases slightly for $KClO_4$. Semi-quantitative analysis of the release behavior of Cl, a representative of the Cl-containing species, was conducted by measuring its peak intensity ($m/z = 35$) of B-$LiClO_4$ and B-$NaClO_4$ upon release relative to B-$KClO_4$ over the 10 ms of collection time. The results displayed in Fig. 3 (c).

A higher intensity of a particular species in the spectra indicates that the average release rate of that species over the collection period is higher. Fig. 3(c) clearly illuminates that the average rates of release of Cl from B/$LiClO_4$ and B/$NaClO_4$ reactions are much higher (~3X) compared to B/$KClO_4$ reaction. During combustion, a higher energy release rate causes rapid increase in temperature, which in turn leads to an increase in the reaction rate. As shown in Fig. 2, B/$LiClO_4$ and B/$NaClO_4$ ignite while B/$KClO_4$ does not, indicating more energy is released from B/$LiClO_4$ and B/$NaClO_4$ than B/$KClO_4$. For B/$LiClO_4$ and B/$NaClO_4$, the significant amount of energy released from the combustion promotes the decomposition of $LiClO_4$ and $NaClO_4$, respectively. Therefore, much more Cl-containing species are released compared to B/$KClO_4$ because decomposition of $KClO_4$ is not enhanced.

Fig. 4 (a) and (b) display the mass spectra of bare metal iodates and B/iodate composites upon rapid heating. The bare metal iodates share the same decomposition behavior, where they mainly release corresponding metal, $O_2$, $I^2$, I and $I_2$, and the intensity of I-containing species from $LiIO_3$ is much higher than $NaIO_3$ and $KIO_3$, as shown in Fig. 4. Intensity of I-containing species increases for all three iodates when B is introduced, however, the extent of the increase is different. Semi-quantitative analysis displayed in Fig. 4 (c) shows that the increase of I release from $LiIO_3$ and $NaIO_3$ is more significant than that of $KIO_3$ when B is added (>2X). As discussed above, a more significant increase in intensity of the species from decomposition of the oxidizer indicates more energy is released from the combustion reaction. Therefore, the mass spectra result suggests B/$LiIO_3$ and B/$NaIO_3$ release more energy than B/$KIO_3$. This is consistent with the ignition test results, where B/$LiIO_3$ and B/$NaIO_3$ ignite while B/$KIO_3$ does not in 1 atm argon.

### 3.3. Thermal behavior under slow heating rate (10 K/min)

This still leaves on the question as to why $KClO_4$ and $KIO_3$ behave differently compared to their Li and Na counterparts in boron ignition. To explore this difference, thermolysis of the metal perchlorates and iodates were carried out with slow heating rate (10 K/min) thermogravimetric-differential scanning calorimetry (TGA-DSC) in an argon environment. The results are shown in Fig. 5 and Fig. 6.

$LiClO_4$ shows previously documented multiple-stepped mass loss that results from dehydration up to 150 °C, a melting endotherm at 248 °C and exothermic decomposition onset at 473 °C [55,56]. $NaClO_4$ shows an endotherm at 306 °C that corresponds to a phase transition from orthorhombic to cubic, a melting endotherm at 467 °C, followed by an exothermic decomposition onset at 542 °C [57,58]. Similarly, $KClO_4$ demonstrates a phase change from rhombic to cubic at 302 °C, a melting process at 610 °C and a decomposition onset at 610 °C [59]. One think that became clear from these results is that there is a temperature gap between the melting and decomposition temperature which we have shown as the shaded area. As the shaded areas indicate, the temperature intervals between melting and decomposition onset are ~225 °C, ~75 °C and ~0 °C for $LiClO_4$, $NaClO_4$ and $KClO_4$, respectively. We believe it is this temperature gap that provides a key to understanding our observations.

Thermolysis results of iodates further support this hypothesis. Iodates demonstrate similar decomposition behaviors to perchlorates, where $LiIO_3$ and $NaIO_3$ decompose about 95 °C and 80 °C above the melting point, respectively, while $KIO_3$ melts and decomposes at about the same temperature, as shown in Fig. 6 [60]. From the proposed hypothesis, as the intervals between melting and decomposition of $LiIO_3$ and $NaIO_3$ are much larger than that of $KIO_3$, it is expected B/$LiIO_3$ and B/$NaIO_3$ to have more violent ignition than B/$KIO_3$. T-Jump ignition test

result matches this expectation and validates the hypothesis (Fig. 2).

### 3.4. Proposed mechanism

As a general rule, all things being equal, one should expect that the more mobile the reactants, the more facile should be the chemistry, assuming all other variables are invariant. As such one might expect then that a reactant that releases an oxidizer fragment would most efficiently react with fuel if it is in intimate contact prior to release of the oxidant. In particular we see from Fig. 5 that $LiClO_4$ particles melt well before decomposing, and thus one might expect wetting of the B nanoparticles to occur before $LiClO_4$ decomposes. Therefore, B nanoparticles have a more facile access to oxidant upon $LiClO_4$ decomposition, which leads to violent ignition. $NaClO_4$ behaves similarly to $LiClO_4$, but its size is larger and melting-decomposition temperature difference is smaller than $LiClO_4$, thus there is less time for melted $NaClO_4$ to surround/wet B nanoparticles before decomposition, resulting in less vigorous ignition. $KClO_4$ is significantly different than either $LiClO_4$ or $NaClO_4$, as its decomposition and melting are concurrent, which means that most of oxidant release occurs in the proximity of B but not necessarily in intimate contact with B, and only those B nanoparticles with intimate contact with $KClO_4$ initially are oxidized efficiently, leading to a barely visible ignition event. This likely is the reason why $KClO_4$ appears to be a poor oxidizer for B. Ignition behavior difference among B/iodates can be explained in the same manner, where $LiIO_3$ and $NaIO_3$ melt and wet the B nanoparticles before decomposing and result in more violent ignition than $KIO_3$, which melts and decomposes concurrently. Although the particles synthesized from ASP for $KIO_3$ are slightly larger than $LiIO_3$ and $NaIO_3$, as shown in Figure S6, the ignition behaviors with B are far too different to be explained by the particle size difference.

Ignition of B/$XClO_4$ and B/$XIO_3$ (X = Li or Na) may also be further facilitated by the added complexity of the interaction between melted $B_2O_3$ and $XClO_4$ or $XIO_3$. Nanoscale B has native $B_2O_3$ shell that melts at 450 °C [9], a temperature that is above the melting temperature, but below the decomposition temperature of $XClO_4$ and $XIO_3$, suggesting that both the oxide shell and $XClO_4$ or $XIO_3$ are melted before the oxidizer decomposition. It is likely that the liquid perchlorates or iodates are partially miscible with melted $B_2O_3$, so the liquid $B_2O_3$ is partially dissolved into the liquid perchlorates or iodates before the decomposition of these oxidizers. This means that the thickness of liquid barrier that retards the B oxidation is reduced and diffusion of oxygen to the boron core or boron to the oxide surface is enhanced, leading to a more violent ignition. While for B/$KClO_4$ and B/$KIO_3$, this effect is negligible since $KClO_4$ and $KIO_3$ have a minimum window between melting and decomposing. These effects are summarized in Fig. 7.

## 4. Conclusions

This study investigates the role of alkali metal perchlorate and iodate type on the ignition behavior of nanoscale B. B/$XClO_4$ and B/$XIO_3$ (X = Li or Na) composites ignite in atmospheric pressure argon while B/$KClO_4$ and B/$KIO_3$ do not. T-Jump TOFMS demonstrates that when B is added, there is a dramatic increase of Cl-containing and I-containing species from $XClO_4$ and $XIO_3$ than $KClO_4$ and $KIO_3$, respectively, which is attributed to the higher amount of heat released from the ignition reaction. TGA/DSC analysis reveals that there is an interval of $\sim$ 225 °C and $\sim$ 75 °C between the melting point and decomposition onset of $LiClO_4$ and $NaClO_4$ respectively, whereas $KClO_4$ melts and decomposes concurrently. Similarly, $LiIO_3$ and $NaIO_3$ decompose $\sim$ 95 °C and $\sim$ 80 °C after melting, respectively, while $KIO_3$ melts and decomposes at about the same temperature, A mechanism emphasizing the difference between melting and decomposition of the oxidizers is proposed to explain the difference in ignition behavior among the B/metal salt-based oxidizer composites. For B/$XClO_4$ and B/$XIO_3$, the larger interval between melting and decomposition renders more time for the oxidizer to melt and surround/wet the nanoscale B before decomposing, providing instant access to oxidant for B nanoparticles that results in vigorous ignition. While for B/$KClO_4$ and B/$KIO_3$, only B nanoparticles that are in intimate contact with $KClO_4$ or $KIO_3$ particles have access to oxygen upon the oxidizer decomposition, resulting in a less likely ignition event.

### Declaration of Competing Interest

The authors declare that they have no known competing financial
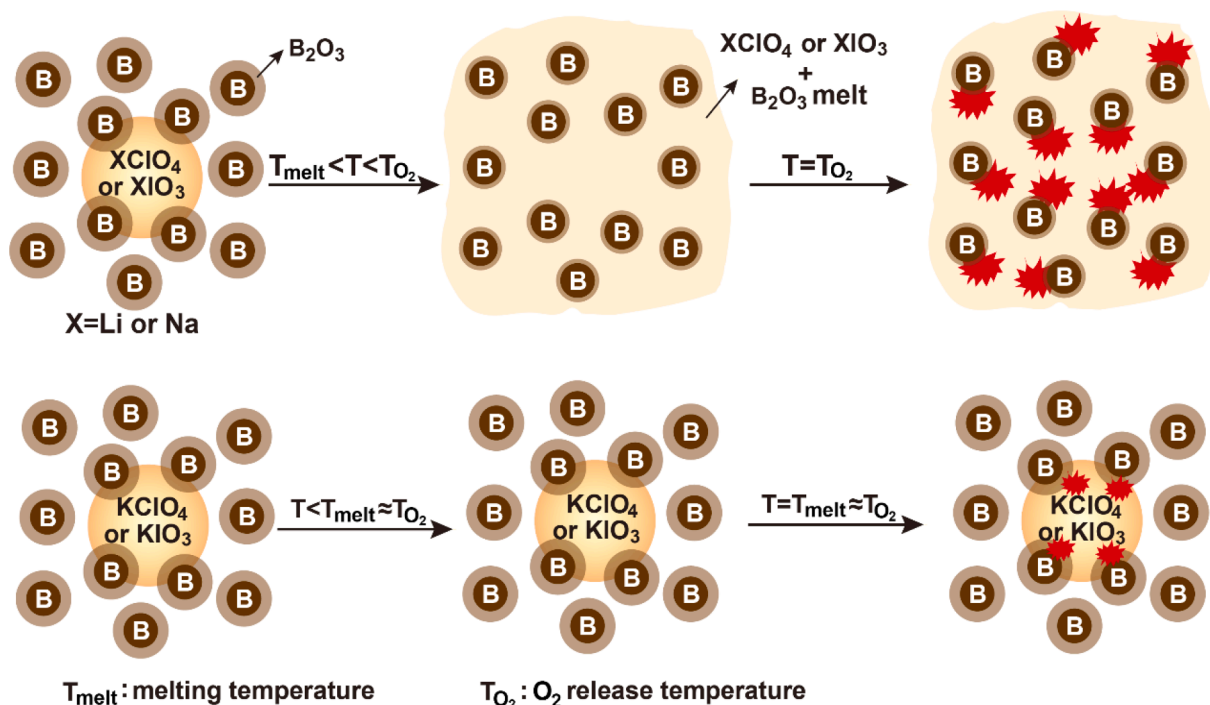


**Fig. 7.** Proposed mechanism for the correlation of the ignition behavior and the difference between melting and decomposition temperatures.

interests or personal relationships that could have appeared to influence the work reported in this paper.

## Acknowledgement

## Appendix A. Supplementary data

Supplementary data to this article can be found online at https://doi.org/10.1016/j.cej.2022.136786.

## References

[1] M.C. Rehwoldt, Y. Yang, H. Wang, S. Holdren, M.R. Zachariah, Ignition of nanoscale titanium/potassium perchlorate pyrotechnic powder: reaction mechanism study, J. Phys. Chem. C. 122 (2018) 10792–10800, https://doi.org/10.1021/acs.jpcc.8b03164.

[2] G.C. Egan, K.T. Sullivan, T.Y. Olson, T.-Y.-J. Han, M.A. Worsley, M.R. Zachariah, Ignition and combustion characteristics of nanoaluminum with copper oxide nanoparticles of differing oxidation state, J. Phys. Chem. C. 120 (2016) 29023–29029, https://doi.org/10.1021/acs.jpcc.6b11081.

[3] S.K. Valluri, M. Schoenitz, E. Dreizin, Bismuth fluoride-coated boron powders as enhanced fuels, Combust. Flame. 221 (2020) 1–10, https://doi.org/10.1016/j.combustflame.2020.07.023.

[4] D.B. Lempert, G.N. Nechiporenko, G.B. Manelis, Energetic capabilities of high-density composite solid propellants containing zirconium or its hydride, Combust. Explos. Shock Waves. 47 (2011) 45–54, https://doi.org/10.1134/S0010508211010060.

[5] F. Xu, G. Nava, P. Biswas, I. Dulalia, H. Wang, Z. Alibay, M. Gale, D.J. Kline, B. Wagner, L. Mangolini, M.R. Zachariah, Energetic characteristics of hydrogenated amorphous silicon nanoparticles, Chem. Eng. J. 430 (2022) 133140.

[6] M.K. King, Ignition and combustion of boron particles and clouds, J. Spacecr. Rockets. 19 (1982) 294–306, https://doi.org/10.2514/3.62256.

[7] C.L. Yeh, K.K. Kuo, Ignition and combustion of boron particles, Prog. Energy Combust. Sci. 22 (1996) 511–541, https://doi.org/10.1016/S0360-1285(96)00012-3.

[8] A. Ulas, K.K. Kuo, C. Gotzmer, Ignition and combustion of boron particles in fluorine-containing environments, Combust. Flame. 127 (2001) 1935–1957, https://doi.org/10.1016/S0010-2180(01)00299-1.

[9] S. Huang, S. Deng, Y. Jiang, X. Zheng, Experimental effective metal oxides to enhance boron combustion, Combust. Flame. 205 (2019) 278–285, https://doi.org/10.1016/j.combustflame.2019.04.018.

[10] W. Ao, Y. Wang, H. Li, J. Xi, J. Liu, J. Zhou, Effect of initial oxide layer on ignition and combustion of boron powder, Propellants Explos. Pyrotech. 39 (2014) 185–191, https://doi.org/10.1002/prep.201300079.

[11] K.-L. Chintersingh, Y. Sun, M. Schoenitz, E.L. Dreizin, Heterogeneous reaction kinetics for oxidation and combustion of boron, Thermochim. Acta. 682 (2019) 178415, https://doi.org/10.1016/j.tca.2019.178415.

[12] H. Krier, R.L. Burton, M.J. Spalding, T.J. Rood, Ignition dynamics of boron particles in a shock tube, J. Propuls. Power. 14 (1998) 166–172, https://doi.org/10.2514/2.5282.

[13] J.L. Gottfried, E.R. Wainwright, S. Huang, Y. Jiang, X. Zheng, Probing boron thermite energy release at rapid heating rates, Combust. Flame. 231 (2021), 111491, https://doi.org/10.1016/j.combustflame.2021.111491.

[14] R.A. Yetter, H. Rabitz, F.L. Dryer, R.C. Brown, C.E. Kolb, Kinetics of high-temperature B/O/H/C chemistry, Combust. Flame. 83 (1991) 43–62, https://doi.org/10.1016/0010-2180(91)90202-M.

[15] K.-L. Chintersingh, M. Schoenitz, E.L. Dreizin, Oxidation kinetics and combustion of boron particles with modified surface, Combust. Flame. 173 (2016) 288–295, https://doi.org/10.1016/j.combustflame.2016.08.027.

[16] D. Liang, J. Liu, Q. Qiu, Nano carbides-mediated acceleration of energy release behavior of amorphous boron during ignition and combustion, Energy Rep. 6 (2020) 1160–1169, https://doi.org/10.1016/j.egyr.2020.05.002.

[17] J. Xi, J. Liu, Y. Wang, D. Liang, J. Zhou, Effect of metal hydrides on the burning characteristics of boron, Thermochim. Acta. 597 (2014) 58–64, https://doi.org/10.1016/j.tca.2014.10.017.

[18] J. Liu, J. Xi, W. Yang, Y. Hu, Y. Zhang, Y. Wang, J. Zhou, Effect of magnesium on the burning characteristics of boron particles, Acta Astronaut. 96 (2014) 89–96, https://doi.org/10.1016/j.actaastro.2013.11.039.

[19] A.G. Korotkikh, I.V. Sorokin, Effect of Me/B-powder on the ignition of high-energy materials, Propellants Explo Pyrotec 46 (11) (2021) 1709–1716.

[20] K.-L. Chintersingh, M. Schoenitz, E.L. Dreizin, Effect of purity, surface modification and iron coating on ignition and combustion of boron in air, Combust. Sci. Technol. 193 (9) (2021) 1567–1586.

[21] K.-L. Chintersingh, M. Schoenitz, E.L. Dreizin, Transition metal catalysts for boron combustion, Combust. Sci. Technol. 193 (8) (2021) 1400–1424.

[22] D. Liang, J. Liu, J. Xiao, J. Xi, Y. Wang, J. Zhou, Effect of metal additives on the composition and combustion characteristics of primary combustion products of B-based propellants, J. Therm. Anal. Calorim. 122 (2015) 497–508, https://doi.org/10.1007/s10973-015-4750-6.

[23] M. Ma, G. Liu, Z. Qin, R. Zhang, Y. Ying, L. Xu, D. Liu, Effects of aluminum addition on flash ignition and combustion of boron nanoparticles, Combust. Flame. 236 (2022), 111762, https://doi.org/10.1016/j.combustflame.2021.111762.

[24] S.A. Hashim, S. Karmakar, A. Roy, Effects of Ti and Mg particles on combustion characteristics of boron–HTPB-based solid fuels for hybrid gas generator in ducted rocket applications, Acta Astronaut. 160 (2019) 125–137, https://doi.org/10.1016/j.actaastro.2019.04.002.

[25] G. Young, K. Sullivan, M.R. Zachariah, K. Yu, Combustion characteristics of boron nanoparticles, Combust. Flame. 156 (2009) 322–333, https://doi.org/10.1016/j.combustflame.2008.10.007.

[26] Q. Song, W. Cao, X. Wei, J. Liu, J. Yuan, X. Li, X. Guo, D. Gao, Laser ignition and combustion characteristics of micro- and nano-sized boron under different atmospheres and pressures, Combust. Flame. 230 (2021), 111420, https://doi.org/10.1016/j.combustflame.2021.111420.

[27] T.-K. Liu, S.-P. Luh, H.-C. Perng, Effect of boron particle surface coating on combustion of solid propellants for ducted rockets, Propellants Explos. Pyrotech. 16 (1991) 156–166, https://doi.org/10.1002/prep.19910160403.

[28] P.R. Deshmukh, H. Lee, Y. Kim, W.G. Shin, Ignition and oxidation performance of SnO2 coated boron particles: A solid fuel for energetic applications, J. Alloys Compd. 886 (2021) 161123.

[29] V. Keerthi, H. Nie, S. Pisharath, H.H. Hng, Combustion characteristics of fluoropolymer coated boron powders, Combust. Sci. Technol. 194 (6) (2022) 1183–1198.

[30] I.-M. Shyu, T.-K. Liu, Combustion characteristics of GAP-coated boron particles and the fuel-rich solid propellant, Combust. Flame. 100 (1995) 634–644, https://doi.org/10.1016/0010-2180(94)00032-N.

[31] Y. Jiang, N.E. Dincer Yilmaz, K.P. Barker, J. Baek, Y. Xia, X. Zheng, Enhancing mechanical and combustion performance of boron/polymer composites via boron particle functionalization, ACS Appl. Mater. Interfaces. 13 (24) (2021) 28908–28915.

[32] J. Xi, J. Liu, Y. Wang, D. Liang, H. Li, J. Zhou, Role of oxalic acid in promoting ignition and combustion of boron: an experimental and theoretical study, Propellants Explos. Pyrotech. 39 (2014) 844–851, https://doi.org/10.1002/prep.201400048.

[33] B. Van Devener, J.P.L. Perez, J. Jankovich, S.L. Anderson, Oxide-free, catalyst-coated, fuel-soluble, air-stable boron nanopowder as combined combustion catalyst and high energy density fuel, Energy Fuels. 23 (2009) 6111–6120, https://doi.org/10.1021/ef900765h.

[34] Y. Hu, X. Wang, J. Zhang, Z. Zhu, X. Ren, Y. Yang, K. Lin, A. Pang, Y. Shuai, Encapsulated boron-based energetic spherical composites with improved reaction efficiency and combustion performance, Chem. Eng. J. 433 (2022) 134478.

[35] J. Piao, L. Deng, Y. Mao, J. Wang, L. Zhang, Promoting the combustion properties of boron powder through in-situ coating, Nano Sel. n/a (n.d.). https://doi.org/10.1002/nano.202100344.

[36] T. Liu, X. Chen, H. Xu, A. Han, M. Ye, G. Pan, Preparation and properties of boron-based nano-B/NiO thermite, Propellants Explos. Pyrotech. 40 (2015) 873–879, https://doi.org/10.1002/prep.201400308.

[37] S.K. Valluri, P.M. Gandhi, M. Schoenitz, E.L. Dreizin, Boron-rich composite thermite powders with binary Bi2O3·CuO oxidizers, Energy Fuels. 35 (12) (2021) 10327–10338.

[38] X. Wang, T. Wu, H. Wang, J.B. DeLisio, Y. Yang, M.R. Zachariah, Boron ignition and combustion with doped δ-Bi2O3: Bond energy/oxygen vacancy relationships, Combust. Flame. 197 (2018) 127–133, https://doi.org/10.1016/j.combustflame.2018.07.015.

[39] H. Wang, H. Ren, L. Yin, Y. Li, X. Wu, High energy release boron-based material with oxygen vacancies promoting combustion, Chem. Eng. J. 430 (2022), 133027, https://doi.org/10.1016/j.cej.2021.133027.

[40] Y. Jiang, A.R. Demko, J. Baek, X. Shi, L. Vallez, R. Ning, X. Zheng, Facilitating laser ignition and combustion of boron with a mixture of graphene oxide and graphite fluoride, Appl. Energy Combust. Sci. 1–4 (2020) 100013, https://doi.org/10.1016/j.jaecs.2020.100013.

[41] M.J. Spalding, H. Krier, R.L. Burton, Boron suboxides measured during ignition and combustion of boron in shocked Ar/F/O2 and Ar/N2/O2 mixtures, Combust. Flame. 120 (2000) 200–210, https://doi.org/10.1016/S0010-2180(99)00082-6.

[42] P. Liu, L. Liu, G. He, Effect of solid oxidizers on the thermal oxidation and combustion performance of amorphous boron, J. Therm. Anal. Calorim. 124 (2016) 1587–1593, https://doi.org/10.1007/s10973-016-5252-x.

[43] Materials Project, (n.d.). https://materialsproject.org/ (accessed December 9, 2021).

[44] W. Zhou, J.B. DeLisio, X. Wang, M.R. Zachariah, Reaction mechanisms of potassium oxysalts based energetic composites, Combust. Flame. 177 (2017) 1–9, https://doi.org/10.1016/j.combustflame.2016.05.024.

[45] T. Wu, A. SyBing, X. Wang, M.R. Zachariah, Aerosol synthesis of phase pure iodine/iodic biocide microparticles, J. Mater. Res. 32 (2017) 890–896, https://doi.org/10.1557/jmr.2017.6.

[46] G. Jian, N.W. Piekiel, M.R. Zachariah, Time-resolved mass spectrometry of nano-Al and Nano-Al/CuO thermite under rapid heating: a mechanistic study, J. Phys. Chem. C. 116 (2012) 26881–26887, https://doi.org/10.1021/jp306717m.

[47] G. Jian, S. Chowdhury, K. Sullivan, M.R. Zachariah, Nanothermite reactions: Is gas phase oxygen generation from the oxygen carrier an essential prerequisite to ignition? Combust. Flame. 160 (2013) 432–437, https://doi.org/10.1016/j.combustflame.2012.09.009.

[48] J.B. DeLisio, X. Hu, T. Wu, G.C. Egan, G. Young, M.R. Zachariah, Probing the reaction mechanism of aluminum/poly(vinylidene fluoride) composites, J. Phys. Chem. B. 120 (2016) 5534–5542, https://doi.org/10.1021/acs.jpcb.6b01100.

[49] M.C. Rehwoldt, Y. Wang, F. Xu, P. Ghildiyal, M.R. Zachariah, High-temperature interactions of metal oxides and a PVDF binder, ACS Appl. Mater. Interfaces. 14 (7) (2022) 8938–8946.

[50] W. Zhou, J.B. DeLisio, X. Wang, G.C. Egan, M.R. Zachariah, Evaluating free vs bound oxygen on ignition of nano-aluminum based energetics leads to a critical reaction rate criterion, J. Appl. Phys. 118 (11) (2015) 114303.

[51] F. Xu, P. Biswas, G. Nava, J. Schwan, D.J. Kline, M.C. Rehwoldt, L. Mangolini, M. R. Zachariah, Tuning the reactivity and energy release rate of I2O5 based ternary thermite systems, Combust. Flame. 228 (2021) 210–217, https://doi.org/10.1016/ j.combustflame.2020.12.047.

[52] W. Ao, Y. Wang, S. Wu, Ignition kinetics of boron in primary combustion products of propellant based on its unique characteristics, Acta Astronaut. 136 (2017) 450–458, https://doi.org/10.1016/j.actaastro.2017.03.002.

[53] Y.I. Vovchuk, A.N. Zolotko, L.A. Klyachko, D.I. Polishchuk, V.G. Shevchuk, Gasification of boron oxide, Combust. Explos. Shock Waves. 10 (1974) 538–540, https://doi.org/10.1007/BF01465287.

[54] T. Yoshida, S. Yuasa, Effect of water vapor on ignition and combustion of boron lumps in an oxygen stream, Proc. Combust. Inst. 28 (2000) 2735–2741, https:// doi.org/10.1016/S0082-0784(00)80694-3.

[55] Application and Research on the Generation of Oxygen from the Decomposition of Lithium Perchlorate, Ship Electronic Engineering. 08 (2012). https://en.cnki.com. cn/Article_en/CJFDTotal-JCGC201208046.htm (accessed April 26, 2021).

[56] Non-isothermal Decomposition Mechanism and Kinetics of LiClO_4 in Nitrogen, Chemical Research in Chinese Universities, 02 (2010). https://www.cnki.com.cn/ Article/CJFDTotal-GHYJ201002033.htm (accessed April 26, 2021).

[57] C.R. Becker, L.J. Currano, W.A. Churaman, C.R. Stoldt, Thermal analysis of the exothermic reaction between galvanic porous silicon and sodium perchlorate, ACS Appl. Mater. Interfaces. 2 (2010) 2998–3003, https://doi.org/10.1021/ am100975u.

[58] D.J. Devlin, P.J. Herley, Thermal decomposition and dehydration of sodium perchlorate monohydrate, React. Solids. 3 (1987) 75–84, https://doi.org/10.1016/ 0168-7336(87)80019-0.

[59] S.M. Pourmortazavi, M. Fathollahi, S.S. Hajimirsadeghi, S.G. Hosseini, Thermal behavior of aluminum powder and potassium perchlorate mixtures by DTA and TG, Thermochim. Acta. 443 (2006) 129–131, https://doi.org/10.1016/j. tca.2005.11.045.

[60] W.M. Haynes, CRC handbook of chemistry and physics, CRC Press, 2014.